Ultrathin Zwitterionic Polymeric Interphases for Stable Lithium Metal Anodes

Sanjuna Stalin[a‡], Pengyu Chen[a‡], Gaojin Li[a‡], Yue Deng[b], Zachary Rouse[b], Yifan Cheng[a], Zhenyuan Zhang[a], Prayag Biswal[a], Shuo Jin[a], Shefford P. Baker[b], Rong Yang[a], Lynden A. Archer[a]

[a]School of Chemical and Biomolecular Engineering, Olin Hall, Cornell University, Ithaca, New York 14853, United States

[b]Department of Materials Science and Engineering, Bard Hall, Cornell University, Ithaca, New York 14853, United States

[‡]These authors contributed equally.

Key Words: Electrodeposition; Chemical Vapor Deposition; Polymers; Coatings; Interfaces

Abstract: Lithium metal electrodeposits in the form of irregular morphological features known as dendrites on planar anode substrates, that lead to rapid battery failure and safety concerns. Due to the highly reducing nature of Li (−3.04 V vs standard hydrogen electrode), a solid electrolyte interphase (SEI) inevitably forms at electrode/electrolyte interface, which regulates the subsequent electrodeposition of Li. Rational design of the chemical, mechanical and ion transport properties of SEI plays important roles in determining the morphology of electrodeposited metals. We report on a novel approach, by using initiated Chemical Vapor Deposition (iCVD), to create ultrathin and conformal polymeric interphases with precise thicknesses in the range (10-500) nm. A zwitterionic polymer was synthesized and mediated the process of lithium electrodeposition. It is found that zwitterionic moieties are able to tune the solvation environment of the lithium cation at the electrode/electrolyte interface enabling compact, planar deposition of the lithium metal. These findings provide new directions for designing ionic polymeric interphases for metal anodes.

Introduction:

Li-ion batteries (LIBs), a technological innovation that was recognized with the Nobel Chemistry Prize in 2019, have and will for the foreseeable future play a decisive role in enabling advances towards carbon neutral operations in a variety of technology sectors. The limited specific energy of LIBs (SE_{LIB}=200-250 Wh kg^{-1}) is known to be a fundamental barrier to the rapid progress in electrification of the transportation sector and to broad-based use of electric power from renewable resources. These limitations have put a spotlight on advances in chemistry that enable rechargeable batteries that employ metals as anodes. Lithium metal batteries stand out among the options for a variety of now well-known reasons.[1-6] The most important is that the Li anode offers a very high theoretical specific capacity of 3,860 mAh g^{-1}, enabling batteries that exceed energy density values

of 500 Wh kg^{-1} when paired with state-of-the-art high-voltage Ni-rich cathodes. These Lithium Metal Batteries (LMBs) are however well-known to be fraught with various challenges posed by complex interfacial phenomena particularly at the metallic anode/electrolyte interface, with impacts electrodeposition morphology, reversibility, and safety of the battery. Due to the highly reactive and reducing nature of alkali metal anodes, a heterogenous corrosion layer, known as the solid electrolyte interphase (SEI), forms on the anode surface due to chemical and electrochemical reactions between the metal and electrolyte components consisting of compounds such as Li_2O, LiF, Li_2O_3 and other semi-carbonates and alkoxides[7,8]. During battery recharge, these heterogenous interphases produce hotspots where preferential lithium electrodeposition occurs, causing lithium to deposit in a non-planar, porous and mossy fashion, loosely termed as dendrites[3] that are detrimental to the safety and long term performance of the cell. Overtime the spontaneously formed SEI may also rupture and reform continuously due to large volume changes at the anode caused by the growing dendrites, consuming more electrolyte and electrochemically active lithium in the process.

Precise control over the composition and properties of the SEI is desired for overcoming the chemical and mechanical instabilities at the electrode/electrolyte interface and thereby achieving stable and high-performance LMBs. The interfacial energy, mechanical properties and spatial variation in physical properties of the SEI has a large influence on Li^+ ion transport rates and redox reaction kinetics that influences nucleation and growth of the metal. Several attempts have been reported towards creation of interphases with controlled properties that would enable planar and non-porous lithium electrodeposits. Approaches including (i) use of electrolyte additives[4–6,9] such as fluoroethylene carbonate, vinylene carbonate, lithium nitrate etc., which may either facilitate or retard electroreduction reactions of other electrolyte components, can be used to fundamentally

alter the composition of the interphase by forming a highly conductive, homogenous and/or mechanically stable SEI; (ii) design of solid/composite electrolytes that exhibit favorable mechanical and ion transport properties that can arrest physical instabilities that lead to dendrite growth[10–16]; (iii) High concentration or localized high concentration electrolytes whereby the cation solvation structure is modified to reduce the activity of solvent molecules and in turn prevent their decomposition products in the SEI [17–19] , or novel design of artificial interphases which tune ion transport and reaction kinetics at the interface while accommodating volume changes[20–27] . Tailoring the electrode/electrolyte interface with polymeric interphases is particularly attractive since the viscoelastic nature of polymers allow them to accommodate high levels of strains and volume changes at the anode.

Various methods and techniques have emerged for forming these conformal polymeric interphases over the past few years. However, most of these approaches involve use of solvents that lead to undesirable surface tension effects which result in coating defects like dewetting, formation of pinholes and other types of non-uniformity, which invariably drive uncontrolled metal deposition and dendrite formation. There is also limited freedom to explore the effect of different chemical functionalities afforded by the polymeric interphase on metal deposition and electrode reversibility due to the constraints imposed by polymer solubility, which is a prerequisite for a polymer to be casted as a coating for anodes. Furthermore, thickness control is critical for artificial interphases. Recent studies show that an optimum thickness value exists for a given electrolyte system, reflecting a balance between the conflicting needs for high surface tension & mechanical forces (e.g. as offered by thick interphases), which enable planar deposition, and the simultaneous need for low interphase resistance and low overpotentials for ion transport (which favors thin interphases)[28,29].

In the midst of the polymer coating technique evolution embodied by the development of the artificial polymeric SEI, initiated chemical vapor deposition (iCVD) appears as a new promising technology[30]. The iCVD is a solvent-free polymerization technique that enables the one-step synthesis and application of functional polymer nanolayers with precisely controlled film thickness and complete retention of chemical functionalities[30,31]. By avoiding solvents and undesirable surface tension effects, the polymer films synthesized via iCVD form uniform and defect-free coverage on a metal substrate. Meanwhile, the absence of residual solvent or other additives prevent undesired side reactions and accumulation of their decomposition products on the metal electrode. Furthermore, the iCVD possesses a rich library of functional monomers (even combination of monomers) that can be employed. This provides access to designer polymer interphases for electrochemical cells with a plethora of precisely controlled physicochemical properties, ranging from viscoelastic linear polymers to stiff highly crosslinked polymers, from superhydrophobic fluoropolymers to hydrophilic zwitterionic polymers[32,33] and hydrogels[34], and from charge-neutral hydrocarbon polymers to polymers affording either charge or both. Previously, we reported that polymeric interphases that contain ionic groups are attractive candidates because of their simultaneously regulate ion transport and provide spatially resolved mechanics that counteract development of deposition hot-spots at a lithium metal anode and enable planar electrodeposition of lithium[28]. Ionic polymers containing tethered cations[35] as well as anions[26] have previously been reported, for example, to prevent ion-polarization at the metal/electrolyte interface and to promote metal deposition at low overpotentials. We hypothesize that polymeric interphases containing zwitterionic moieties are attractive candidates for artificial interphases for two main reasons: (i) Zwitterionic polymers contain a high concentration of cationic and anionic groups along their backbone, which can assist in the dissociation and

conduction of ions at the electrode/electrolyte interface, while maintaining overall charge neutrality; (ii) Zwitterionic salts have been previously shown to be useful electrolyte additives in polymeric electrolytes to improve ionic conductivity[36].

A robust artificial interphase that is able to tune the redox kinetics at the electrode surface and morphology of the electrodeposited lithium is thus highly desirable as a scalable path towards high energy density lithium metal batteries. In this study, we report on the synthesis of polymeric coatings formed via initiated chemical vapor deposition (iCVD) and study their impact on lithium electrodeposit morphology and reversibility. Based on that rationale and leveraging the advantages of the all-dry iCVD technique, we create ultrathin zwitterionic polymeric interphases and experimentally demonstrate their exceptional ability to enable planar lithium electrodeposition. The effect of the molecular structure of the zwitterionic moieties and their composition in the polymer interphases on electrochemical stability and reversibility is investigated first to ensure the polymer itself does not form additional reduction products and a secondary SEI. After screening for chemical and electrochemical stability, zwitterionic polymer interphases with the most promising electrochemical features were selected for in-depth Li deposition and reversibility studies in half cells and full cells. NMR and voltammetry experiments supported by a theoretical linear stability analysis show that electrochemically stable interphases are not only effective at promoting Li electrode reversibility, but they do so by altering the coordination environment of the lithium cation. This modifies the redox reaction kinetics at the electrode surface favorably, resulting in stable lithium electrodeposition in both early and late stages of growth.

Results and Discussion:

The schematic diagram reported in **Figure 1** summarizes the synthesis scheme used to create zwitterionic polymers considered in this study. During the iCVD process, polymer coatings were created via a free-radical polymerization mechanism. Monomers, argon carrier gas (not shown due to its chemical inertness), and initiator- tert-butylperoxide (TBPO) are introduced into a vacuum chamber that also contained the substrates to be coated placed on a cooled stage (20-30°C). The purpose of stage cooling is two-fold. First, it protects thermally labile substrates. Second, it enables physisorption of monomers, which typically follows the BET isotherm. Free radicals generated via thermolytic cleavage of the initiator, TBPO, initiate polymerization of physiosorbed monomers. Cleavage is produced by passing the TBPO through an array of metal filaments, resistively heated to 230ºC, which supplies the energy for generating the radicals in the vapor phase. Free-radical polymerization subsequently proceeds upon surface impingement of the radicals, following an Eley–Rideal mechanism[37].

The chemical structure of the different monomers that form the co-polymers of interest in the present study are reported in **Figure S1**. We specifically investigated zwitterionic polymers derivatized from pyridine, imidazole and ammonium-based copolymers. Pyridine, imidazole and ammonium monomers containing a vinyl or acrylate functional group were chosen as they were commercially available. Ionic liquids have been reported previously to have varying levels of cationic stability limits based on the structure of the cation, with ammonium and piperidinium based ionic liquids exhibiting higher stability limits, compared to pyridinium and imidazolium ionic liquids[38]. We aim to similarly understand the cathodic stability limits for our zwitterionic copolymers systematically and screen for electrochemically stable copolymers.

The zwitterionic polymer coatings used in the present work were created using a two-step method reported in our previous work[39–42], where the tertiary nitrogen in poly(4-vinylpyridine-co-divinylbenzene)[poly(4VP-co-DVB)], poly(1-vinylimidazole-co-divinylbenzene)[poly(VI-co-DVB)] and poly(dimethylaminoethyl acrylate-co-divinylbenzene) [poly(DMAEMA-co-DVB)] was converted to a quaternized sulfobetaine group in a vapor-based derivatization step using 1,3-propanesultone, following the iCVD step. Reaction and deposition conditions used for the synthesis are summarized in **Table** S1.

Molecular structures of the as-deposited copolymers and the derivatized zwitterionic polymers were confirmed using Fourier transform infrared (FTIR) (**Figure 1b**). In the FTIR spectrum of poly(4-vinylpyridine-co-divinylbenzene), the characteristic vibrations of pyridine ring were present at 1598, 1556, 1461 and 1416 cm^{-1}. The peaks at 1497, 1284, 1083, 744 and 663 cm^{-1} are contributed to various vibrational modes of the imidazole ring. The C=O and $N(CH_3)_2$ groups in poly(DMAEMA-co-DVB) were confirmed by the 1730 cm^{-1} and 2821 cm^{-1} peaks. After derivatization, a strong absorbance peak at 1035 to 1039 cm^{-1} was detected, indicating a successful obtainment of the sulfobetaine zwitterionic moieties in the copolymers, which is attributed to the symmetric stretching of the SO_3^- group. In addition, X-ray Photoelectron Spectroscopy (XPS) of N 1s high resolution scans were conducted on the zwitterionic films. The nitrogen signals shifts from around 399.5 eV, corresponding to tertiary amine (pyridine N, imidazole N and amine N), to around 401.5 eV, corresponding to the quaternary amine (pyridinium, imidazolium and ammonium), indicating successful and high degree of derivatization. (**Figure 1c**)

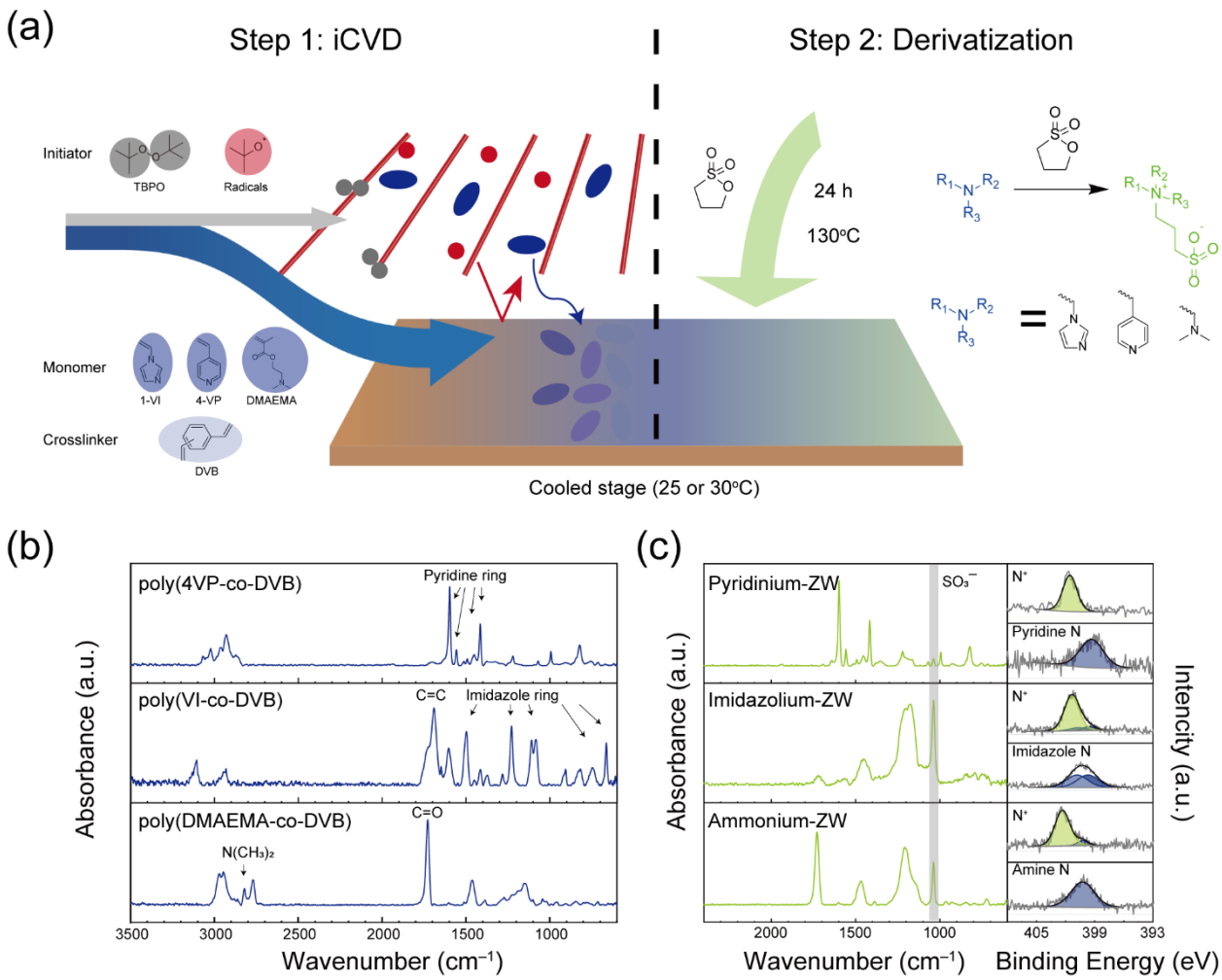

Figure 1: Schematic illustration of the fabrication of zwitterionic polymeric interphases and structural characterization. (a) Schematic illustration of the fabrication of zwitterionic polymeric interphases. Step 1: iCVD precursor polymer film (25°C for poly(4VP-co-DVB) and 30°C for poly(VI-co-DVB) and poly(DMAEMA-co-DVB)); Step 2: derivatization. (b) FTIR spectra of poly(4VP-co-DVB), poly(VI-co-DVB) and poly(DMAEMA-co-DVB)). (c) FTIR spectra and XPS of N 1s of the zwitterionic films.

We first characterized the physical stability of the polymer coatings on a copper substrate, used as the current collector for subsequent lithium deposition studies. Delamination of the polymer

coating from the current collector/metallic substrate is possible due to interaction with the bulk liquid electrolyte and swelling of the formed polymer. In order to characterize the physical stability of the coatings on the copper substrates, NMR analysis was performed for a liquid electrolyte sample before and after exposure to the coated substrates for a period of 24 hours. Any dissolution or delamination would be detected in the bulk electrolyte post exposure. **Figure S2** reports the C^{13}, Li^{7} and F^{19} NMR spectra of the electrolyte. The results show that no additional peaks and shifts were observed, indicating that the coatings are in fact stable on the copper substrate on exposure to the liquid electrolyte.

Previously, we reported that an optimum thickness value exists for an ex-situ synthesized polymer interphase and that this optimum is dependent upon specific polymer properties such as ion diffusivity and shear modulus. The existence of such an optimum is important because it underscores the importance of capturing the delicate balance between resistance and elasticity, specifically for polymers with low Li^{+} ion diffusivity values[28], when fabricating artificial interphases for metal electrodes. To that end, we deposited a series of zwitterionic polymers with different thickness values of 10,50,100 and 500 nm for electrodeposition experiments under galvanostatic conditions to understand the optimum thickness value for the zwitterionic polymers. The thickness of the as-deposited polymer coatings was characterized by ellipsometry and the data was fitted by the Cauchy-Urbach model (**Figure S3**). The uniformity and conformality of the ultrathin polymer films were also investigated. As shown in **Figure S4**, SEM images are reported for the 10-nm coating on copper foil because the analysis demands the most stringent requirements for uniformity. The pristine copper foil exhibits a rough surface morphology with characteristic scratches from top left to bottom right. Such features are perfectly maintained after 10-nm polymer coatings are formed, irrespective of the coating polymer chemistry. Atomic Force Microscopy

(**Figure S5**) measurements show that the root-mean-square (RMS) roughness is 0.11± 0.09 nm for silicon wafer, 0.06± 0.05 nm for polymer coating before derivatization and 0.14± 0.11 nm for polymer coating after derivatization, implying that the polymer coatings do not add extra surface features before and after the derivatization reaction. Mechanical properties of the polymer films were investigated using nanoindentation with 1 μm thick deposited polymer films on wafers. Due to the slow deposition rate of the imidazole monomer, only interphases composed of the DMAEMA zwitterionic copolymer and the 4VP zwitterionic copolymers were investigated. Results reported in **Figure S6** show that the indentation modulus is approximately 10 GPa and that the values increase after the derivatization reaction. The measured indentation modulus is higher than the indentation modulus of Lithium metal (~9 GPa)[43].

To evaluate the effectiveness of the coatings in regulating Li electrodeposition morphology, we studied the morphology of Li deposited from a typical 1M $LiPF_6$ EC/DMC/DEC electrolyte under galvanostatic conditions (current density = 1 mA/cm^2). A fixed capacity (1 mAh/cm^2) of Li was used for all experiments. Analysis of scanning electron microscopy (SEM) images of the deposits reported in **Figure S7** show for interphase thickness values 10,50,100 and 500 nm that Li typically deposits under the zwitterionic polymer coatings. The results show further that lithium electrodeposits under the 10nm coating showed the most consistent and stable morphology without grain boundaries compared to other thickness values. For further experiments, we therefore maintained the interphase coating thickness at 10 nm in all cases.

The intrinsic electrochemical stability of artificial metal/electrolyte interphases is an important determinant of their durability inside a battery. Electrochemical stability of the polymeric coatings can be evaluated through cyclic voltammetry measurements at a moderately slow scan rate of 0.1 mV/s as reported in **Figure 2(a)**. The coated substrates were scanned from 2.5 V to -0.2V and the

current evolution through plating and stripping of lithium metal measured. No additional current peaks were observed, compared to the uncoated copper substrate. However, the current magnitude was reduced by a large amount, indicating suppression of redox reactions at the electrode. Although cyclic voltammetry at moderately low scan rates is a reliable way of characterizing electrochemical stability of components in liquid electrolytes, comparatively slow ion transport rates and kinetics of degradation reactions in the solid state are known benefits of solid-state electrolytes[14], which could be problematic in the present case because they would skew results towards higher cathodic stability limits. In order to decouple the stability from transport limitations and kinetic effect, we performed chronoamperometry measurements coupled with electrochemical impedance spectroscopy. 1M $LiPF_6$ in EC/DMC/DEC was used as the electrolyte and lithiated LTO ($Li_4Ti_5O_{12}$) employed as the counter and reference electrode, since the SEI contribution from LTO is low to negligible and any increase in interfacial resistance can be attributed to the formation and growth of an SEI on the working electrode. The coated or uncoated substrate was held at different reductive potentials vs Li/Li^+ for until the reductive currents reach steady state; the impedance of the cells was subsequently measured. Representative raw EIS spectra at different reductive potentials for the ammonium based zwitterionic polymer coated substrate are shown in **Figure 2(b)**.

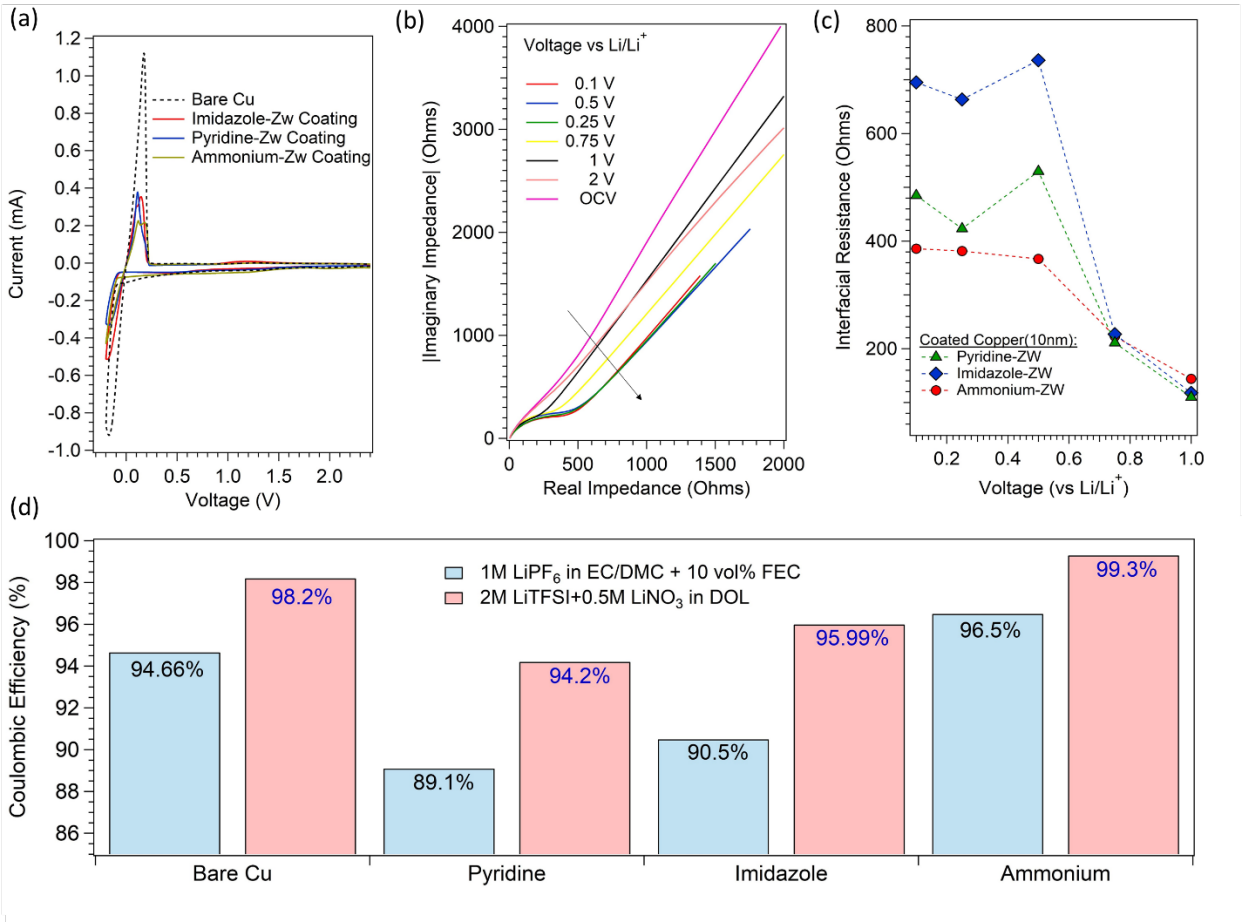

Figure 2: Screening iCVD polymers for electrochemical stability: (a) Cyclic Voltammetry of bare and coated copper electrodes at a slow scan rate of 0.1 mV/s, (b) Representative Nyquist plots for the LTO|| Copper (Ammonium-ZW coated) cells post chronoamperometry measurements at different reductive potentials vs Li/Li$^+$, (c) Interfacial impedance values obtained from fitting the Nyquist plots with an equivalent circuit model (d) Coulombic Efficiency values of the different working electrodes when paired with two kinds of electrolytes, obtained using the Aurbach protocol

Evidence for an interface formation, characterized by a semicircle in the EIS spectrum, is clearly observed for reductive potentials below 1V. Fitting the spectra with an appropriate model allows us to decouple the bulk, interfacial, and charge transfer contributions. The model fitting details are

reported in **Figure S8** and **Table S2** and the extracted interfacial impedance for the three coatings is reported in **Figure 2(c).** While the ammonium based zwitterionic polymer coated substrate reaches a steady state impedance value beyond a certain potential, the imidazole and pyridine-based coating show much higher values of impedance that do not reach a steady state value as the reduction potential is decreased. These results correlate well with the coulombic efficiency measurements reported in **Figure 2(d).** Reversibility was accessed by pairing the coated substrates with carbonate- and ether-based electrolyte systems commonly used in LMBs. It is clear that while the pyridine and imidazole-based coatings show lower reversibility compared to the uncoated electrode, the ammonium based zwitterionic polymer enhances reversibility in both the electrolyte systems studied. Based on our observations, we believe that the cations of the zwitterionic copolymers impact electrochemical stability similarly to that of ionic liquids.

Surface analysis using XPS of electrodes cycled in a baseline carbonate electrolyte (1 M $LiPF_6$ in EC/DMC/DEC), without any additives, shed light on the decomposition products formed on the surface after stripping and plating lithium. XPS spectra for the four electrodes of interest after cycling are reported in **Figure S9**. In general, organic compounds, such as fluorocarbons and inorganic salts such as carbonates and LiF, are observed on the surface of all samples. The N(1S) spectra show no nitrogen species on the uncoated electrode, as expected. On the pyridine- or imidazole-based zwitterionic coatings, the N(1s) scans reveal higher concentration of tertiary amine species compared to quaternary nitrogen species. The ammonium-based coating however showed predominately quaternary ammonium species. While imidazole contains both quaternary and tertiary nitrogen, post the derivatization reaction, our results hint at potential degradation of the organic nitrogen cation in the imidazole- and pyridine-based coatings, consistent with the chronoamperometry and coulombic efficiency results (**Figure 2**). These results align well with

computational and experimental studies that highlight the superior reductive stability of aliphatic cations compared to cations derived from aromatic structures[44,45]. It has been reported that the main route to reduction in aromatic cations like imidazolium occurs at the C2 position, while in aliphatic cations like ammonium, the most accessible route is through the breaking of C-N bond. After screening the zwitterionic copolymers for electrochemical stability, we chose the derivatized poly(DMAEMA-co-DVB) coating for the following studies to evaluate its impact on lithium electrodeposition stability and morphology.

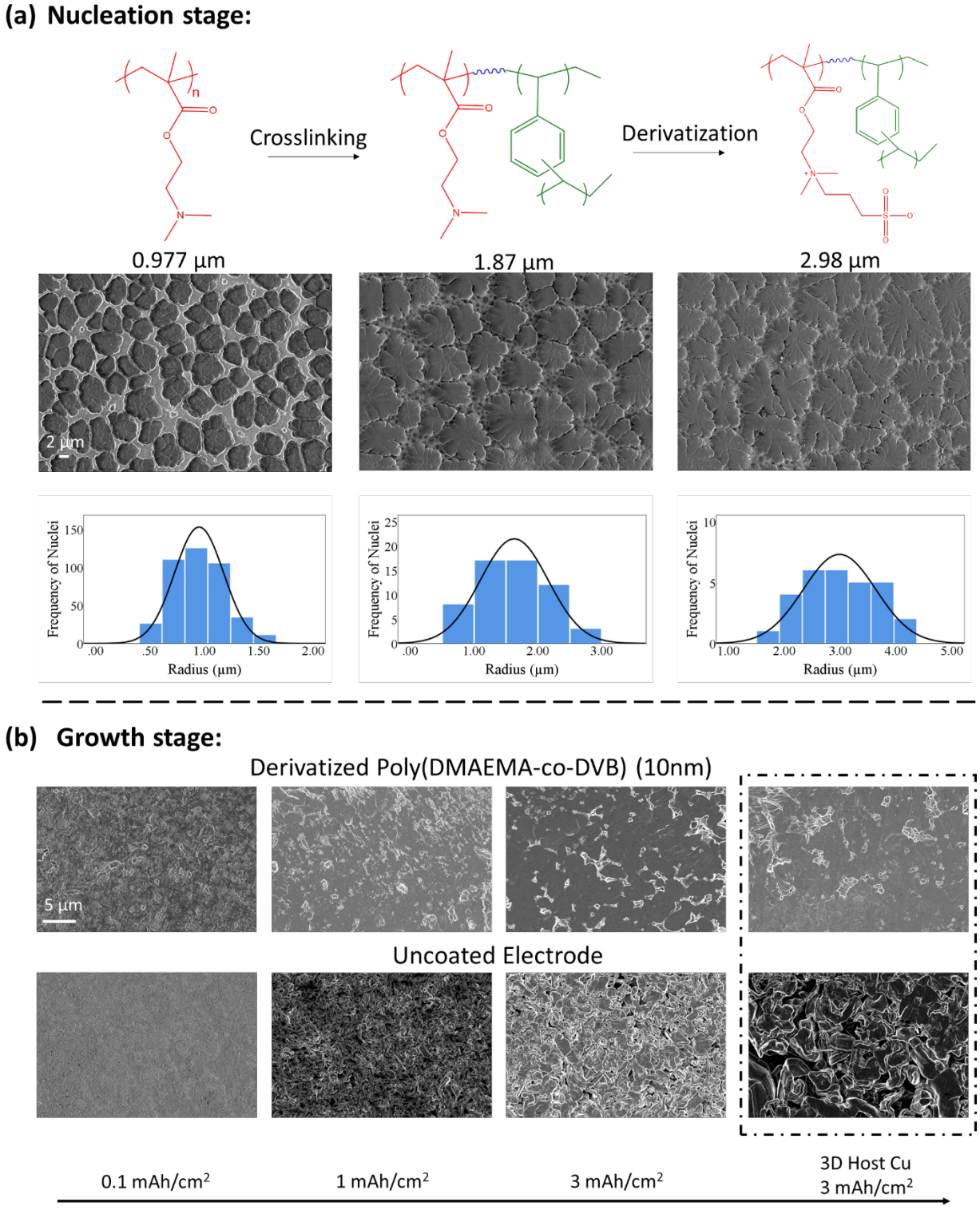

Figure 3:Impact of zwitterionic interphase on Lithium electrodeposit morphology: (a) Morphology of lithium electrodeposits formed in the early nucleation stages on polished stainless steel

substrates coated with 10nm thick poly(DMAEMA), poly(DMAEMA-co-DVB) and derivatized poly(DMAEMA-co-DVB) artificial solid-electrolyte interphases. The polymer interphases were synthesized using iCVD on polished stainless steel current collectors to eradicate substrate roughness effects and the images were analyzed using Image J. The histograms of analyzed images are reported below the SEM images. Values for the mean nucleate sizes achieved are reported below the structures of the respective polymer repeat units. (b)Deposit morphology of lithium electrodeposits on coated (top row) and uncoated (bottom row) electrodes for different capacities during the long-time, growth stage. A 10nm thick zwitterion polymer coating was applied to the current collector substrates used for the CE measurements in Fig. 2d, including copper foils and 3D microporous copper electrodes (right most in box). All experiments utilized a standard 1M $LiPF_6$ electrolyte with 10% FEC additive.

To understand the effect of the zwitterionic copolymer on early stage nucleation of lithium electrodeposits, polished stainless steel (RMS roughness ~ 9 nm) current collectors were coated with poly(DMAEMA), poly(DMAEMA-co-DVB) and their derivatized products (*i.e.*, zwitterionic polymers) to assess the separate effects of crosslinking and of zwitterionic moieties on the nucleation process. Polished stainless steel current collectors are used to eliminate any influence of substrate roughness. In our experiments, a fixed capacity of 0.1 mAh/cm^2 Li was deposited on the coated substrates under galvanostatic conditions (1 mA/cm^2). **Figure 3 (a)** reports the SEM images of the lithium nuclei formed under the three polymer coatings studied, along with the histograms reporting the distribution of nucleus sizes of the analyzed images. As observed from the extracted average nucleus size from image analysis, crosslinking alone leads to an increase in nucleus size and a more planar morphology, while incorporation of zwitterionic groups further

increases the nucleus size and leads to a flatter morphology. It is possible that crosslinking reduced the dissolution of poly(DMAEMA) into the bulk electrolyte while also increasing the mechanical modulus of the polymer. Higher mechanical modulus and increase in diffusivity of ions have been previously reported to lead to an increase in nucleus size[28,29], correlating well with our results.

To understand the effect of the zwitterionic polymer coating at higher Li capacities on more practical copper current collectors, lithium electrodeposits with capacities ranging from 0.1 to 3 mAh/cm^2 were imaged on coated and uncoated substrates as reported in **Figure 3(b)**. Non-uniform, needle like deposition is observed in the case of the uncoated electrode. In contrast, the polymer coated substrate enabled planar deposition for all capacities with no obvious grain boundaries. The effects of the interphases on Li electrodeposition in/on a 3D microporous copper current collector was also investigated. 3D copper current collectors are considered attractive as they can host higher capacities compared to planar substrates. However, the rough edges in such a microporous substrate typically leads to dendritic Li deposition. As seen in **Figure 3(b)**, the polymer coating leads to more closely packed, non-granular deposits compared to the uncoated electrode, indicating that the zwitterionic polymer coating is as effective alleviate the physical irregularities in the porous current collector.

In order to elucidate the mechanism by which the zwitterionic polymer enables planar deposition, the effect of the polymer on the ion transport and reaction kinetics at the electrode/electrolyte interface were first analyzed. It is specifically important to understand the effect of the zwitterionic moieties on solvation and desolvation of lithium ions. Zwitterionic groups have previously been shown to coordinate with lithium ions and increase their dissociation from the polymer backbone in polyelectrolytes[36]. In order to study the effect and extent of participation of the zwitterionic

groups in the lithium solvation shell, we performed a series of NMR experiments with baseline liquid electrolytes, the electrolyte with DMAEMA monomer additive and the electrolyte with the derivatized DMAEMA monomer (N-(3-Sulfopropyl)-N-(methacryloxyethyl)-N,N-dimethylammonium betaine or DMAPS) additive. **Figure 4(a)** reports the Li^7 NMR spectra of the electrolytes with and without the monomer additives. Compared to the reference sample, the baseline electrolyte showed an upfield shift of close to 0.3 ppm, indicating a strong increase in electron density around the solvated Li^+ ion. In order to rule out the effect of magnetic drifts of the instrument, we also measured the chemical shifts of the reference sample before and after the experiment. Reported in **Figure S10**, the results show that there was no change in the peak shifts, indicating that all upfield shifts observed during the experiment were solely due to the difference in the ion solvation environment of the Li^+ ions.

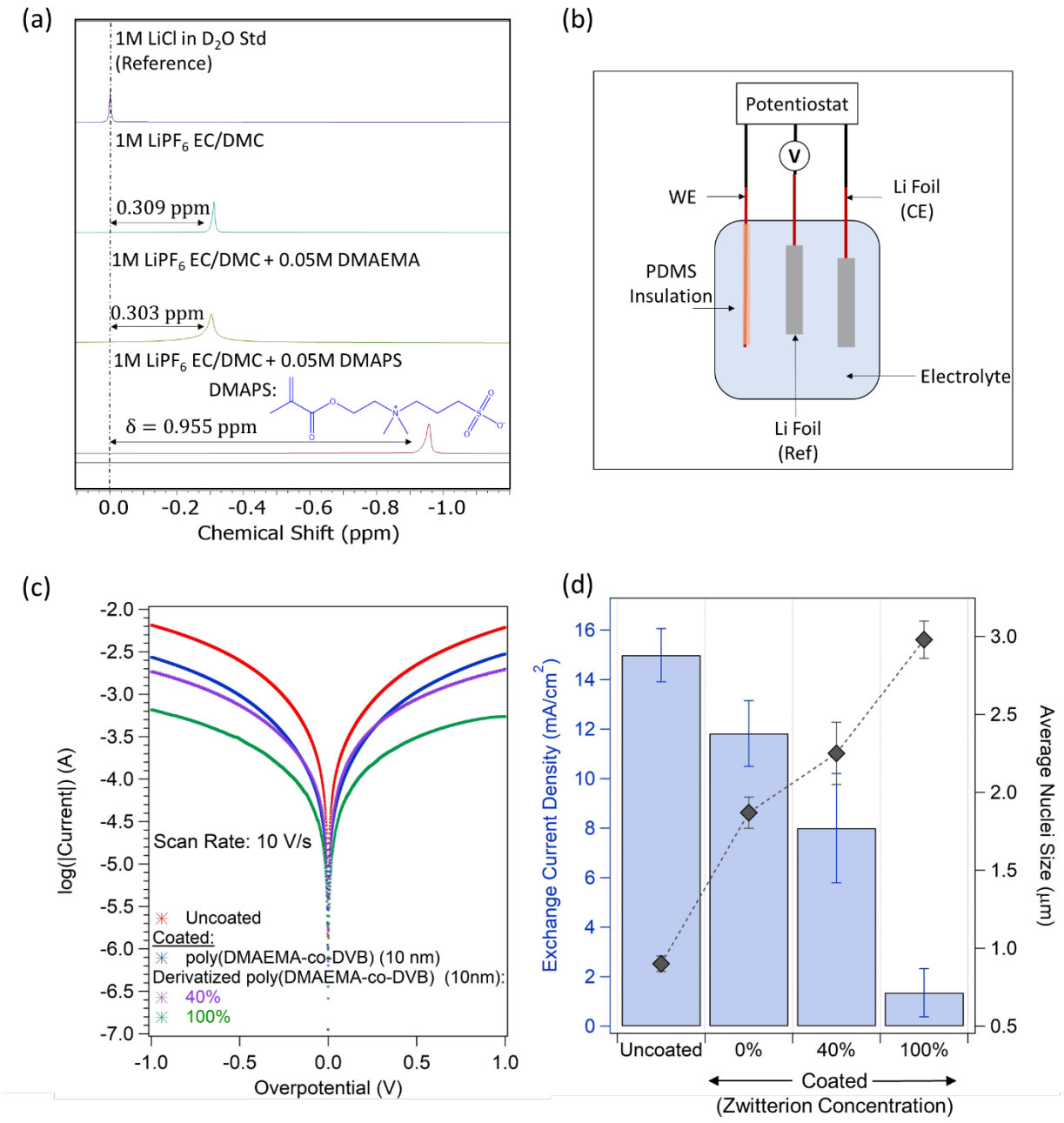

Figure 4:Effect of polymeric interphase on redox reaction kinetics (a) NMR spectra of reference and electrolyte with and without DEA and DMAPS additive (b) Setup for exchange current density measurments (c) Tafel plots obtained from voltammetry measurments performed at a high scan rate of 10V/s (d) Extracted exchange current density values from the tafel plots

The NMR analysis of the electrolyte with 0.05M of DMAEMA showed chemical shifts that are close to those of the baseline electrolyte, with no noticeable difference in the upfield shift values. This indicates that there is negligible variation in the solvation environment of the Li^+ ions. Upon addition of 0.05M DMAPS, an upfield shift of around ~0.955 ppm is observable, indicating substantial change in the solvation environment of the lithium cations induced specifically by the zwitterionic groups. To investigate this effect further,[7]Li NMR experiments were performed on electrolytes with different concentrations of DMAPS, the results are reported in **Figure S11**. It is clear that the upfield shift increases systematically as the concentration of DMAPS increases. Previously, similar NMR analysis was utilized to understand solvent-ion interactions and contact pair formations in concentrated electrolytes and electrolytes with oligomer additives and co-solvents[19,20,46]. The upfield shift in general also implies an increase in solvation energy of the Li^+ ion due to stronger ion-pairing, coordination, or strong electrostatic interactions between the solvated ions. While this provides evidence for active participation of the zwitterionic moieties in the solvation environment of the ions, it also has implications for the reaction kinetics at the electrode interface. Increase in ion-pairing and solvation energy reduces the activity coefficient of Li^+ ions and lowers the exchange current density according $J_o = K_o ne(c_o^* c_e^{*n})^{(1-\alpha)} c_R^{*\alpha}[\frac{(\gamma_O \gamma_e^n)^{(1-\alpha)}\gamma_R^\alpha}{\gamma_\Psi}]$, derived from the generalized Butler- Volmer equation for concentrated solutions[43] where J_o is exchange current density, K_o is the equilibrium rate constant, n is the number of electrons transferred in reaction, c_o^* is the concentration of oxidized species (cations) ,α is the cathodic charge transfer coefficient, γ_O is the oxidized species activity coefficient, γ_R is the reduced state activity coefficient, and γ_Ψ is the transition state activity coefficient. This chemical potential in turn impacts the exchange current density, J_o, which is the equilibrium reaction rate at the electrode. A vast number of literature reports indicate that lowering the exchange current

density at a metal electrode leads to more planar and uniform metal electrodeposition morphology[3,48–50]. Our NMR results thus suggest that the potential mechanism by which the zwitterionic copolymer coating enables smooth electrodeposition is through increased interaction and coordination with the lithium ions and potentially impacting reaction kinetics at the interface.

To evaluate this hypothesis further, we designed a three-electrode electrochemical cell, illustrated in **Figure 4(b)**, which allows the exchange current densities at the electrodes with/without the artificial zwitterionic polymer SEI to be quantified. The cell consisted of lithium counter and reference electrodes and a thin copper wire insulated throughout by a PDMS coating and Kapton except for the tip, drastically reducing the exposed active surface area. A small cross-sectional area is required for accurately measuring exchange current densities in order to ensure that the electrode reactions are kinetically controlled, and not limited by mass transport effects due to the electrolyte and SEI. Working electrodes with small cross-sectional areas are specifically required to sustain such large scan rates (10 V/s) as they have small cell time constants[51]. The exchange current densities were measured for the base copper, copper electrode coated with poly(DMAEMA-co-DVB) and the copper electrode coated the derivatized copolymer. SEI coatings with variable fractions of zwitterions were created by controlling the reaction temperature and time (for the high fraction, the reaction condition is 130°C for 24 h whereas for the low fraction, it is 50°C for 1 h.), in the second step of the synthesis protocol. The concentration of zwitterions/derivatized groups in the coatings was determined by atomic analysis using high resolution XPS surface scans (**Figure S12**). The Tafel plots obtained from these studies are reported in **Figure 4(c)** and the extracted J_o values provided in **Figure 4(d)**. The exchange current density drops nominally in the presence of the coating and drops further in the presence of zwitterionic groups, with lower values for higher

concentration of zwitterions in the coating. This verifies our hypothesis that the zwitterionic groups reduce the rate of reaction kinetics at the electrode surface and stabilize the deposition process.

Figure S13 reports SEM image of lithium electrodeposits during early stages of nucleation (0.1 mAh /cm^2) on polished stainless steel current collectors coated with the copolymer containing 40% of zwitterions. . It is clear that the average nuclei sizes for electrodeposits under each of the polymeric interphase increase consistently with increasing zwitterion concentration and decreasing exchange current density, (reported in Figure 4(d)), validating the stabilizing effect of the zwitterions at the interface.

Based on the above experimental evidence, we next analyze the mechanism by which the zwitterionic polymer interphases stabilizes electrodeposition at a metal electrode. We've previously reported a linear stability analysis that involves first perturbing the electrode surface with non-planar deposits (dendrite nucleates) and analyzing conditions in the bulk electrolyte or at an interphase that result in the initial perturbations growing (unstable) or not growing (stable)[3,52]. In the present case, the linear stability analysis considers two main effects: (i) the influence of the interphase in decreasing the exchange current density at the electrode surface; and (ii) the ability of a zwitterionic polymer interphase to decrease the cation activity. The first of the two effects has been discussed in previous literature using linear stability analysis and nucleation theory[53,54]. The second has not and is the main analytical contribution of the present study.

We solve for the growth rate σ of perturbations on a planar electrode surface under a one-dimensional ion diffusion using the same procedure reported in our earlier work[28]. In the context of electrodeposition we are only interested in modes with wave-lengths below the inter-electrode spacing, L, meaning that we only seek solutions for σ in the so-called high wavenumber ($kL>>1$) limit.[53,54] In this limit, it is straightforward to show that σ is an analytical function:

$$\sigma = kv_m \frac{\frac{J}{F}\left(\frac{C_s}{C_0}(1+\frac{|z^-|}{z^+\alpha_c})A_c+A_a\right)-2|z^-|\frac{C_sD^+v_m\Gamma}{RT}(\frac{C_s}{C_0}A_c+A_a)k^2}{\frac{C_s}{C_0}(1+\frac{|z^-|}{z^+\alpha_c})A_c+A_a+\frac{2|z^-|C_sFD^+}{J_0}k} \quad (1)$$

where $A_c = \alpha_c e^{\frac{\alpha_c z^+ F\Phi_s}{RT}}$ and $A_a = \alpha_a e^{\frac{-\alpha_a z^+ F\Phi_s}{RT}}$, wher $\alpha_c = \alpha_a = 0.5$ are the coefficients of the cathodic and anodic reactions on the electrode surface, $v_m = 13.3cm^3/mol$ is the molar volume of the lithium metal, $\Gamma = 1.716\,J/m^2$ is the surface tension of lithium metal, $z^+ = -z^- = 1$ are the valance of the ions, $D^+ = 10^{-6}\ cm^2/s$ is the bulk ion diffusivity, $C_0 = 1M$ is the salt concentration, $C_s = C_0 - JL/(4D^+FC_0)$ is the base state ion concentration on the electrode surface, $L = 25\ \mu m$ is the interelectrode distance, the base state overpotential Φ_s is explicitly solved by the Butler-Volmer condition $J = J_0(\frac{C_s}{C_0}e^{\frac{\alpha_c z^+ F\Phi_s}{RT}} - e^{-\frac{\alpha_a z^+ F\Phi_s}{RT}})$ and J_0 is the exchange current density. Equation (1) is valid for the underlimiting cases ($J < J_{lim} = 4D^+FC_0$/L=150 mA/cm^2), the growth rate for the limiting current cases has a very similar expression and can be found in literature[53,54].

The growth rate σ then depends on the wavenumber of the perturbation k and the applied current J. The first term in the numerator of Equation 1 is positive, meaning that it destabilizes the deposition by causing non-planar perturbations (bumps) to grow. The second term is negative and therefore has the opposite effect — it stabilizes the deposition primarily through the effect of surface tension to constrain the growth of smaller scale deposits. Taken together the two contributions means that electrodeposition of cations is always unstable at small k and stable at large k. **Figure 5(a)** plots the growth rate as a function of wavenumber at different exchange current densities. For $J_0 \gg J_{lim}$, the ion deposition is limited by the transport process and equation (1) reduces to $\sigma = kv_m(\frac{J}{F} - \frac{2z^+|z^-|}{z^++|z^-|}\frac{C_sD^+v_m\Gamma}{RT}k^2)$. For $J_0 \ll J_{lim}$, the ion deposition is limited by chemical process and the growth rate $\sigma = \frac{v_mJ}{2C_sD^+F}\left(\frac{J}{F}(\frac{\alpha_c}{|z^-|}+\frac{1}{z^+}) - \frac{2\alpha_cC_sD^+v_m\Gamma}{RT}k^2\right)$ is also

independent of J_0. The wavelength of the most unstable mode defines the deposit length scale $\lambda_{max} = 1/k_{max}$. In **Figure 5(b)**, the effect of reducing the exchange current density on the nucleation size is more pronounced at a low applied current. At $J = 0.01J_{lim}$, the nuclear size increases about 4.5 times from $a = 4\,\mu m$ for $J_0 \gg J_{lim}$ to $a = 18\,\mu m$ for $J_0 \ll J_{lim}$. At $J = 0.9J_{lim}$, it increases about 1.6 times from $a = 0.14\,\mu m$ to $a = 0.22\,\mu m$. These results are in the same range of values as the experimental measurements.

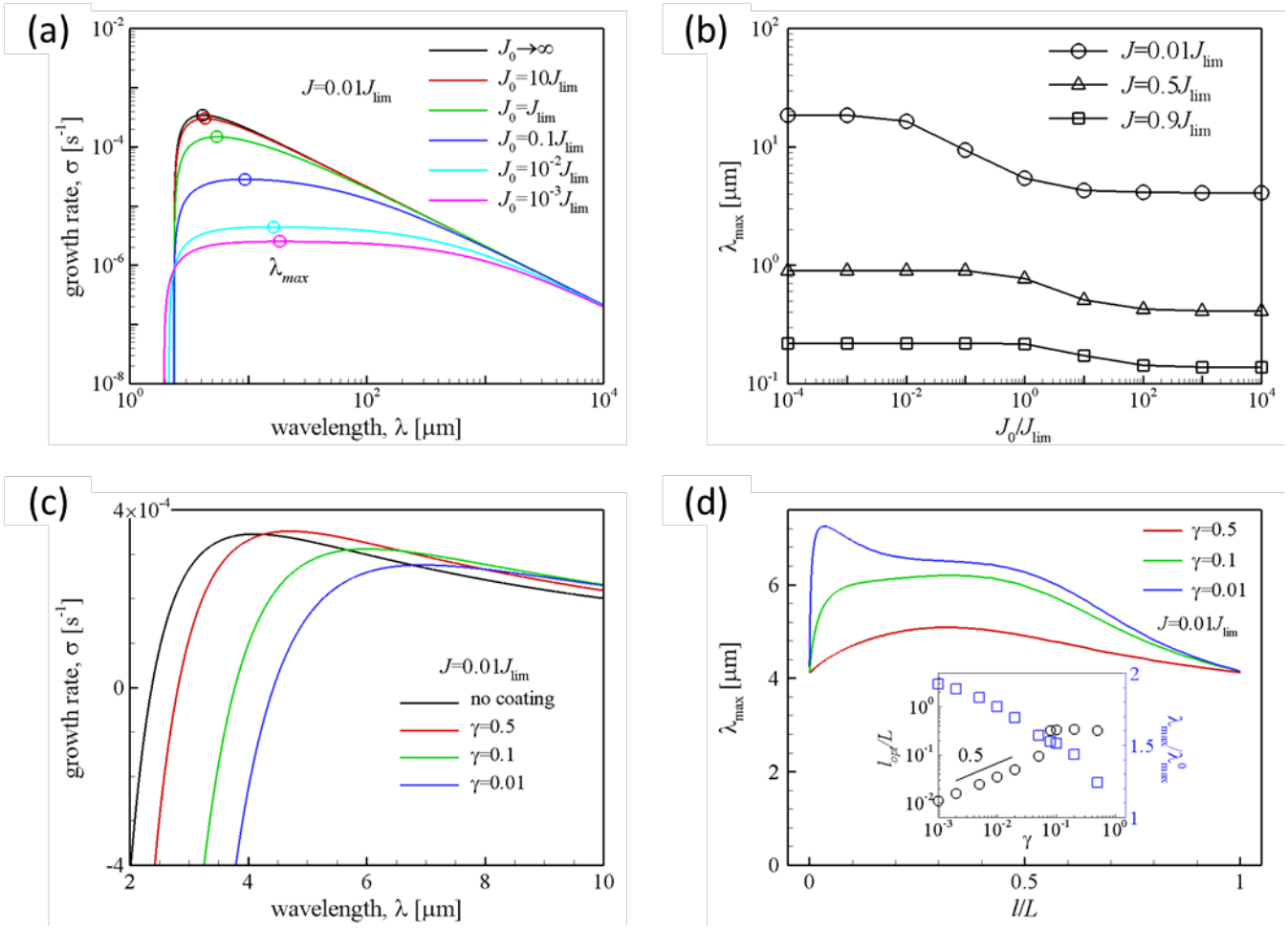

Figure 5 (a) Dependence of growth rate on the wavelength (analogous to Lithium deposit length scale) at $J = 0.01J_{lim}$, Circles show the wavelength of the most unstable mode. (b) Dependence of the wavelength of the most unstable mode on the exchange current density for different applied current densities (c) Dependence of growth rate on the wavelength of perturbation in an electrolyte

without and with polymer coating of thickness l=0.1L. (d) Dependence of the wavelength of the most unstable mode on the thickness of the polymer coating. The inset shows the optimal thickness of the polymer layer l_{opt}/L and the ratio of nucleate size $\lambda_{max}/\lambda_{max}^0$ compared to the no polymer case at different ion activity coefficients.

In order to understand the effect of ion activity and diffusivity on the deposition, we consider the stability of an electrode surface covered by a thin polymer coating layer of thickness l. Inside the polymer region, the cation and anion have activity coefficients $\gamma^{\pm}$. The electrolyte is assumed as an ideal solution in which the activity coefficient is unity. The diffusivity of the ions inside the polymer and electrolyte are $D_p^{\pm}$ and $D_e^{\pm}$, respectively. At the polymer/electrolyte interface, continuity of chemical potential and flux of ions are applied. At the electrode surface, we assume the exchange current density is high ($J_0 \gg J_{lim}$) to focus on the ion activity. The detailed analysis is provided in the supporting material. For a perturbation of high wavenumber ($kL \gg 1$), its growth rate is:

$$\sigma = kv_m \frac{JRT\left(D_p^+ - D_e^+\gamma\right) + D_e^+\left(JRT - \frac{2z^+|z^-|}{z^+ + |z^-|}FC_sD_p^+\Gamma v_m k^2\right)[\gamma\cosh(kl) + \sinh(kl)]}{D_e^+ FRT[\cosh(kl) + \gamma\sinh(kl)]} \quad (2)$$

where $\gamma = \gamma_1\gamma_2$ is the effective activity coefficient of the ion, $\gamma_1 = (\gamma^+)^{\frac{|z^-|}{|z^-|+z^+}}(\gamma^+)^{\frac{z^+}{|z^-|+z^+}}$ is the weighted geometric average of the activity coefficients, $\gamma_2 = e^{\Delta\Phi_\theta}$ is the coefficient caused by the difference of the total reference potentials in the two regions, $\Delta\Phi_\theta = |z^-|(\Phi_{\Theta,p}^+ - \Phi_{\Theta,e}^+) + z^+(\Phi_{\Theta,p}^- - \Phi_{\Theta,e}^-)$,and $\Phi_\Theta^\pm$ is the reference potential, p and e stand for polymer and electrolyte regions. For $l \to 0$, the growth rate reduces to $\sigma = \frac{D_p^+}{D_e^+}kv_m\left(\frac{J}{F} - \frac{2z^+|z^-|}{z^+ + |z^-|}\frac{\gamma C_s D_e^+ v_m \Gamma}{RT}k^2\right)$ with $C_s \approx$

$\frac{C_0 - JL/(4D_e^+ FC_0)}{r}$, and for $l \to L$, i.e., the polymer completely replacing the bulk electrolyte, $\sigma = kv_m(\frac{J}{F} - \frac{2z^+|z^-|}{z^+ + |z^-|}\frac{C_s D_p^+ v_m \Gamma}{RT}k^2)$ recovers the no coating case.

Figure 5(c) shows the growth rate of the perturbation in an electrolyte without and with polymer coating of thickness $l = 0.1L$ and $D_p^+ = D_e^+$. Compared to the influence of changing the exchange current density, reducing the ion activity has a relatively weak effect on the growth rate of the perturbation while it increases wavelength of the most unstable perturbation significantly, i.e., the deposit length scale. **Figure 5(d)** shows the dependence of λ_{max} on the thickness of the polymer coating. At a fixed ion activity, there exists an optimum coating thickness to render the largest nucleation size. For example, at $\gamma = 0.01$, the nucleation size increases from $\lambda_{max} = 4\ \mu m$ (no coating) to the maximum value of $\lambda_{max} = 7.3\ \mu m$ at $l = 0.03L$. The numerator in equation (2) has two terms: the first term is the Mullins-Sekerka destabilizing effect of forming a new solid phase, the second term represents a stabilizing effect due to surface tension. Decreasing the activity increases both terms, and the competition of its contributions leads to an optimum effect of overall stabilization. The inset shows that at small activity γ, the optimal thickness of the polymer layer scales as $l_{opt} \sim \gamma^{0.5}$, showing that even a vanishingly thin layer of polymer coating of low ion activity is effective in increasing the deposit length scale size-it almost doubles at small ion activities. This result is qualitatively consistent with our experiment results, where the optimal thickness of the zwitterionic polymer coating 10 nm is much smaller than the interelectrode distance (~25um) and the nuclei size increases from 1 um to 2um by crosslinking (see figure 3).

Finally, to evaluate the practical relevance of the zwitterionic polymeric interphase in batteries, we first performed strip plate experiments in Li||Cu half cells. A capacity of 1 mAh/cm^2 was deposited on coated/uncoated copper foils and coulombic efficiency was measured with 1M $LiPF_6$ in EC/DMC/DEC as electrolyte with 10% FEC. The coulombic efficiency values and voltage

profiles are reported in **Figure 6(a)** and **6(b)**. It is clear that both the reversibility and lifetime of the Cu foils coated with the ultrathin zwitterionic polymers is greatly enhanced. Additionally, we also created NCM 622 (Capacity~3 mAh/cm^2) || Lithiated Copper full cells and studied their cycling behaviors under galvanostatic conditions. The anode used for these cells was created by lithiating copper current collectors (with/without the polymer coatings) to achieve anodes with Li capacity equal to that of the cathode (3 mAh/cm^2)-a N:P ratio of around 1. It is worth noting that this is a more aggressive mode of testing the efficiency of full cells since there is an intrinsic porosity for the lithium formed via deposition as opposed to store-bought thin lithium anode. An LiTFSI-LiBOB based dual salt electrolyte with $LiPF_6$ additive, that is known to form a stable cathode electrolyte interphase was chosen, in order to understand the effects of the SEI alone in cycling stability. **Figure 6(c)** reports the capacity and coulombic efficiency as a function of cycle number and **Figure 6(d)** reports the voltage profiles for the first cycle after formation and 25^{th} cycle. The capacity retention in the full cells employing coated electrodes is superior to the uncoated case while also maintaining stable coulombic efficiency values, consistent with our previous measurements and results. Additionally, it can be seen that the overpotential between the charge and discharge profiles significantly increase for the uncoated electrode over time in comparison to the coated anode, reflective of reduced electrolyte and lithium metal consumption in the coated electrode. The appropriate protocol for evaluating full cell performance with simple electrolytes requires vapor depositing these zwitterionic polymer directly on thin lithium metal anodes (20-50 μm) and experiments are currently underway for performing iCVD on such reactive substrates.

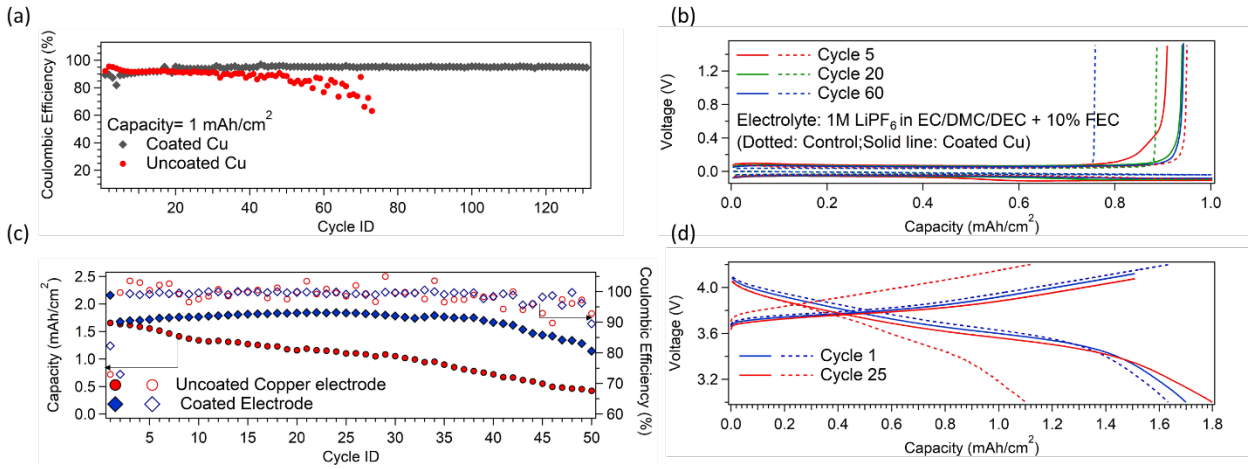

Figure 6: Reversibility of lithium metal anodes with zwitterionic interphase: (a) Coulombic efficiency of Li||Cu half cells for coated (solid) and uncoated (dotted) copper anodes (b) Voltage profiles for the two half cells (c) Cycling results of NCM 622||Lithiated Cu (N:P-1:1) for coated and uncoated copper anodes (d) Voltage profiles for the two systems demonstrating higher capacity fade in cell with uncoated copper electrode.

Conclusions

In conclusion, we utilized a versatile iCVD technique to deposit ultrathin zwitterionic copolymer films as protective coatings on current collectors to stabilize lithium electrodeposition. Through chronoamperometry and impedance measurements, it was found that the chemical functionalities, specifically the organic cations of the zwitterionic polymers, had a significant influence on electrochemical stability. The deposit morphology during early and late stages of growth was significantly more planar under the influence of the iCVD zwitterionic coatings. NMR experiments supported by a theoretical linear stability analysis indicate that the zwitterions actively participate in the solvation environment of the cation, thereby reducing the cation activity and in turn the exchange current density at the anode. Further investigation into functional groups that can tune the cationic activity at the electrode/electrolyte surface can improve the design of polymeric interphases for alkali metal electrodes.

Acknowledgements:

The research was supported by the National Science Foundation, Partnerships for Innovation Program under award # IIP-1919013 and National Institute of Health under award # NIHDC016644. The work made use of materials characterization facilities in the Cornell Energy Systems Institute (CESI), Cornell Center for Materials Research (CCMR), and the Cornell University NMR Facility. CCMR is supported by the National Science Foundation MRSEC program (award number: DMR-1719875) and the NMR facility is supported in part through NSF award number CHE1531632.

Conflicts of Interest:

The authors declare no conflict of interests.

References:

(1) Lin, D; Liu, Y.; Cui, Y. Reviving the lithium metal anode for high-energy batteries. *Nature Nanotechnology*. **2017**, *12*, 194-206

(2) Cheng, X.-B.; Zhang, R.; Zhao, C.-Z.; Zhang, Q. Toward Safe Lithium Metal Anode in Rechargeable Batteries: A Review. *Chem. Rev.* **2017**, *117*, 10403–10473

(3) Tikekar, M. D.; Choudhury, S.; Tu, Z.; Archer, L. A. Design Principles for Electrolytes and Interfaces for Stable Lithium-Metal Batteries. *Nature Energy*. 2016, **1**, 16114

(4) Ding, F.; Xu, W.; Graff, G. L.; Zhang, J.; Sushko, M. L.; Chen, X.; Shao, Y.; Engelhard, M. H.; Nie, Z.; Xiao, J.; Liu, X.; Sushko, P. V.; Liu, J.; Zhang, J. G. Dendrite-Free Lithium Deposition via Self-Healing Electrostatic Shield Mechanism. *J. Am. Chem. Soc.* **2013**, *135* (11), 4450–4456

(5) Choudhury, S.; Archer, L. A. Lithium Fluoride Additives for Stable Cycling of Lithium Batteries at High Current Densities. *Adv. Electron. Mater.* **2015**, *2*, 1500246

(6) Zheng, J.; Engelhard, M. H.; Mei, D.; Jiao, S.; Polzin, B. J.; Zhang, J. G.; Xu, W. Electrolyte Additive Enabled Fast Charging and Stable Cycling Lithium Metal Batteries. *Nat. Energy* **2017**, *2*, 17012

(7) Wu, H.; Jia, H.; Wang, C.; Zhang, J.G.; Xu, W. Recent Progress in Understanding Solid Electrolyte Interphase on Lithium Metal Anodes. *Adv. Energy Mat.* 2021, 1, 2003092

(8) Cheng, X.B.; Zhang, R.; Zhao, C.Z.; Wei, F.; Zhang, J.G.; Zhang, Q. A Review of Solid Electrolyte Interphases on Lithium Metal Anode. *Adv. Sci.* 2016, 3, 1500213

(9) Choudhury, S.; Tu, Z.; Stalin, S.; Vu, D.; Fawole, K.; Gunceler, D.; Sundararaman, R.; Archer, L. A. Electroless Formation of Hybrid Lithium Anodes for Fast Interfacial Ion Transport. *Angew. Chemie - Int. Ed.* **2017**, *56* (42), 13070–13077

(10) Pang, Q.; Zhou, L.; Nazar, L. F. Elastic and Li-Ion–Percolating Hybrid Membrane Stabilizes Li Metal Plating. *Proc. Natl. Acad. Sci. U. S. A.* **2018,** *115 (49),* 12389-12394

(11) Duan, H.; Yin, Y. X.; Shi, Y.; Wang, P. F.; Zhang, X. D.; Yang, C. P.; Shi, J. L.; Wen, R.; Guo, Y. G.; Wan, L. J. Dendrite-Free Li-Metal Battery Enabled by a Thin Asymmetric Solid Electrolyte with Engineered Layers. *J. Am. Chem. Soc.* **2018**, *140* (1), 82–85

(12) Fu, C.; Venturi, V.; Kim, J.; Ahmad, Z.; Ells, A. W.; Viswanathan, V.; Helms, B. A. Universal Chemomechanical Design Rules for Solid-Ion Conductors to Prevent Dendrite Formation in Lithium Metal Batteries. *Nature Materials* **2020**, 19, 758–766

(13) Khurana, R.; Schaefer, J. L.; Archer, L. A.; Coates, G. W. Suppression of Lithium Dendrite Growth Using Cross-Linked Polyethylene/Poly(Ethylene Oxide) Electrolytes: A New Approach for Practical Lithium-Metal Polymer Batteries. *J. Am. Chem. Soc.* **2014**,

136 (20), 7395–7402

(14) Stalin, S.; Johnson, H. E. N.; Biswal, P.; Vu, D.; Zhao, Q.; Yin, J.; Abel, B. A.; Deng, Y.; Coates, G. W.; Archer, L. A. Achieving Uniform Lithium Electrodeposition in Cross-Linked Poly(Ethylene Oxide) Networks: "Soft" Polymers Prevent Metal Dendrite Proliferation. *Macromolecules* **2020,** *53(13)*, 5445–5454

(15) Schaefer, J. L.; Yanga, D. A.; Archer, L. A. High Lithium Transference Number Electrolytes via Creation of 3-Dimensional, Charged, Nanoporous Networks from Dense Functionalized Nanoparticle Composites. *Chem. Mater.* **2013**, *25* (6), 834–839

(16) Zhao, Q.; Stalin, S.; Zhao, C. Z.; Archer, L. A. Designing Solid-State Electrolytes for Safe, Energy-Dense Batteries. *Nat. Rev. Mater.* **2020**, *5*, 229–252

(17) Qian, J.; Henderson, W. A.; Xu, W.; Bhattacharya, P.; Engelhard, M.; Borodin, O.; Zhang, J. G. High Rate and Stable Cycling of Lithium Metal Anode. *Nat. Commun.* **2015**, *6*, 6362

(18) Yu, L.; Chen, S.; Lee, H.; Zhang, L.; Engelhard, M. H.; Li, Q.; Jiao, S.; Liu, J.; Xu, W.; Zhang, J. G. A Localized High-Concentration Electrolyte with Optimized Solvents and Lithium Difluoro(Oxalate)Borate Additive for Stable Lithium Metal Batteries. *ACS Energy Lett.* **2018**, *3* (9), 2059–2067

(19) Ren, X.; Chen, S.; Lee, H.; Mei, D.; Engelhard, M. H.; Burton, S. D.; Zhao, W.; Zheng, J.; Li, Q.; Ding, M. S.; Schroeder, M.; Alvarado, J.; Xu, K.; Meng, Y. S.; Liu, J.; Zhang, J. G.; Xu, W. Localized High-Concentration Sulfone Electrolytes for High-Efficiency Lithium-Metal Batteries. *Chem* **2018**, *4(8),* 1877-1892

(20) Amanchukwu, C. V.; Kong, X.; Qin, J.; Cui, Y.; Bao, Z. Nonpolar Alkanes Modify Lithium-Ion Solvation for Improved Lithium Deposition and Stripping. *Adv. Energy Mater.* **2019**, *9(41)*, 1902116

(21) He, M.; Guo, R.; Hobold, G. M.; Gao, H.; Gallant, B. M. The Intrinsic Behavior of Lithium Fluoride in Solid Electrolyte Interphases on Lithium. *Proc. Natl. Acad. Sci. U. S. A.* **2020**, *117* (1), 73–79

(22) Gao, Y.; Yan, Z.; Gray, J. L.; He, X.; Wang, D.; Chen, T.; Huang, Q.; Li, Y. C.; Wang, H.; Kim, S. H.; Mallouk, T. E.; Wang, D. Polymer–Inorganic Solid–Electrolyte Interphase for Stable Lithium Metal Batteries under Lean Electrolyte Conditions. *Nat. Mater.* **2019**, *18*, 384–389

(23) Lopez, J.; Pei, A.; Oh, J. Y.; Wang, G. J. N.; Cui, Y.; Bao, Z. Effects of Polymer Coatings on Electrodeposited Lithium Metal. *J. Am. Chem. Soc.* **2018**, *140* (37), 11735–11744

(24) Liu, K.; Pei, A.; Lee, H. R.; Kong, B.; Liu, N.; Lin, D.; Liu, Y.; Liu, C.; Hsu, P. chun; Bao, Z.; Cui, Y. Lithium Metal Anodes with an Adaptive "Solid-Liquid" Interfacial Protective Layer. *J. Am. Chem. Soc.* **2017**, *139(13)*, 4815–4820

(25) Yu, Z.; Mackanic, D. G.; Michaels, W.; Lee, M.; Pei, A.; Feng, D.; Zhang, Q.; Tsao, Y.; Amanchukwu, C. V.; Yan, X.; Wang, H.; Chen, S.; Liu, K.; Kang, J.; Qin, J.; Cui, Y.; Bao, Z. A Dynamic, Electrolyte-Blocking, and Single-Ion-Conductive Network for Stable Lithium-Metal Anodes. *Joule* **2019**, *3(11)*, 2761-2776

(26) Tu, Z.; Choudhury, S.; Zachman, M. J.; Wei, S.; Zhang, K.; Kourkoutis, L. F.; Archer, L. A. Designing Artificial Solid-Electrolyte Interphases for Single-Ion and High-Efficiency Transport in Batteries. *Joule* **2017**, *1* (2), 394–406

(27) Choudhury, S.; Stalin, S.; Vu, D.; Warren, A.; Deng, Y.; Biswal, P.; Archer, L. A. Solid-State Polymer Electrolytes for High-Performance Lithium Metal Batteries. *Nat. Commun.* **2019**, *10* (1), 1–8

(28) Stalin, S.; Tikekar, M.; Biswal, P.; Li, G.; Johnson, H. E. N.; Deng, Y.; Zhao, Q.; Vu, D.;

Coates, G. W.; Archer, L. A. Designing Polymeric Interphases for Stable Lithium Metal Deposition. *Nano Lett.* **2020,** *20(8)*, 5749–5758

(29) Kong, X.; Rudnicki, P. E.; Choudhury, S.; Bao, Z.; Qin, J. Dendrite Suppression by a Polymer Coating : A Coarse-Grained Molecular Study. *Adv. Funct. Mater.* **2020**, *1910138*, 1–10

(30) Shen, B. H.; Wang,S ; Tenhaeff., W.E. Ultrathin conformal polycyclosiloxane films to improve silicon cycling stability. *Sci. Adv.* **2019**, *5(7),* eaaw4856

(31) Donadt, T. B.; Yang, R. Vapor-Deposited Biointerfaces and Bacteria: An Evolving Conversation. *ACS Biomater. Sci. Eng.* **2020**, *6(1),* 182–197

(32) Yang, R.; Goktekin, E.; Gleason, K. K. Zwitterionic Antifouling Coatings for the Purification of High-Salinity Shale Gas Produced Water. *Langmuir* **2015**, *31(43)*, 11895–11903

(33) Yang, R.; Goktekin, E.; Wang, M.; Gleason, K. K. Molecular Fouling Resistance of Zwitterionic and Amphiphilic Initiated Chemically Vapor-Deposited (ICVD) Thin Films. *J. Biomater. Sci. Polym. Ed.* **2014**, *25,* 1687-1702

(34) Cheng, Y.; Khlyustova, A.; Chen, P.; Yang, R. Kinetics of All-Dry Free Radical Polymerization under Nanoconfinement. *Macromolecules* **2020,** *53(24)*, 10699–10710

(35) Huang, Z.; Choudhury, S.; Gong, H.; Cui, Y.; Bao, Z. A Cation-Tethered Flowable Polymeric Interface for Enabling Stable Deposition of Metallic Lithium. *J. Am. Chem. Soc.* **2020,** *142(51)*, 21393–21403

(36) Tiyapiboonchaiya, C.; Pringle, J. M.; Sun, J.; Byrne, N.; Howlett, P. C.; MacFarlane, D. R.; Forsyth, M. The Zwitterion Effect in High-Conductivity Polyelectrolyte Materials. *Nat. Mater.* **2004** , *3,* 29–32

(37) Gleason, K. K. *CVD Polymers: Fabrication of Organic Surfaces and Devices*; **2015**, 1-12

(38) Hayyan, M.; Mjalli, F. S.; Hashim, M. A.; AlNashef, I. M.; Mei, T. X. Investigating the Electrochemical Windows of Ionic Liquids. *J. Ind. Eng. Chem.* **2013** ,*19(1),* 106-112

(39) Yang, R.; Gleason, K. K. Ultrathin Antifouling Coatings with Stable Surface Zwitterionic Functionality by Initiated Chemical Vapor Deposition (ICVD). *Langmuir* **2012** ,*28(33)*, 12266–12274

(40) Yang, R.; Xu, J.; Ozaydin-Ince, G.; Wong, S. Y.; Gleason, K. K. Surface-Tethered Zwitterionic Ultrathin Antifouling Coatings on Reverse Osmosis Membranes by Initiated Chemical Vapor Deposition. *Chem. Mater.* **2011**, 23(5), 1263–1272

(41) Yang, R.; Jang, H.; Stocker, R.; Gleason, K. K. Synergistic Prevention of Biofouling in Seawater Desalination by Zwitterionic Surfaces and Low-Level Chlorination. *Adv. Mater.* **2014** ,*26(11)*, 1711-1718

(42) Yang, R.; Moni, P.; Gleason, K. K. Ultrathin Zwitterionic Coatings for Roughness-Independent Underwater Superoleophobicity and Gravity-Driven Oil-Water Separation. *Adv. Mater. Interfaces* **2015**, *2(1),* 1400489

(43) Herbert, E. G.; Hackney, S. A.; Dudney, N. J.; Sudharshan Phani, P. Nanoindentation of High-Purity Vapor Deposited Lithium Films: The Elastic Modulus. *J. Mater. Res.* **2018**, *33*, 1335–1346

(44) Li, Q.; Jiang, J.; Li, G.; Zhao, W.; Zhao, X.; Mu, T. The electrochemical stability of ionic liquids and deep eutectic solvents. *Sci. China.* **2016**, *59,* 571-577

(45) Tian, Y.H.; Goff, G.S; Runde, W.H; Batista, E.R. Exploring Electrochemical Windows of Room-Temperature Ionic Liquids: A Computational Study. *J. Phys. Chem. B.* **2012**, *116(39),* 11943-11952

(46) Wang, Q.; Yang, C.; Zhang, Y.; Yang, J.; Wu, K.; Hu, C.; Lu, J.; Liu, W.; Zhou, H. Surface-Based Li+ Complex Enables Uniform Lithium Deposition for Stable Lithium Metal Anodes. *ACS Appl. Energy Mater.* **2019**, *2* (7), 4602–4608

(47) Bazant, M. Z. Theory of Chemical Kinetics and Charge Transfer Based on Nonequilibrium Thermodynamics. *Acc. Chem. Res.* **2013**, *46(5)*, 1144–1160

(48) Enrique, R. A.; DeWitt, S.; Thornton, K. Morphological Stability during Electrodeposition. *MRS Commun.* **2017,** *7*, 658–663

(49) Shi, F.; Pei, A.; Vailionis, A.; Xie, J.; Liu, B.; Zhao, J.; Gong, Y.; Cui, Y. Strong Texturing of Lithium Metal in Batteries. *Proc. Natl. Acad. Sci. U. S. A.* **2017,** *114 (46)*, 12138-12143

(50) Sadd, M. Insight into the Critical Role of Exchange Current Density on Electrodeposition Behavior of Lithium Metal. *Adv. Energy Mater.* **2021**, *2003301*, 1–11

(51) Boyle, D. T.; Kong, X.; Pei, A.; Rudnicki, P. E.; Shi, F.; Huang, W.; Bao, Z.; Qin, J.; Cui, Y. Transient Voltammetry with Ultramicroelectrodes Reveals the Electron Transfer Kinetics of Lithium Metal Anodes. *ACS Energy Lett.* **2020,** 5(3), 701–709

(52) Tikekar, M. D.; Archer, L. A.; Koch, D. L. Stabilizing Electrodeposition in Elastic Solid Electrolytes Containing Immobilized Anions. *Sci. Adv.* **2016**, *2* (7), e1600320

(53) Nielsen, C. P.; Bruus, H. Morphological Instability during Steady Electrodeposition at Overlimiting Currents. *Phys. Rev. E - Stat. Nonlinear, Soft Matter Phys.* **2015**, *92*, 052310

(54) Pei, A.; Zheng, G.; Shi, F.; Li, Y.; Cui, Y. Nanoscale Nucleation and Growth of Electrodeposited Lithium Metal. **2017,** *17(2)*, 1132–1139